



ELSEVIER

Available online at [www.sciencedirect.com](http://www.sciencedirect.com)

SCIENCE @ DIRECT®

Physica B 338 (2003) 274–283

PHYSICA B

[www.elsevier.com/locate/physb](http://www.elsevier.com/locate/physb)

# Critical behavior of transport in sea ice

K.M. Golden\*

*Department of Mathematics, University of Utah, 155 S 1400 E RM 233, Salt Lake City, UT 84112-0090, USA*

---

## Abstract

Geophysical materials such as sea ice, rocks, soils, snow, and glacial ice are composite media with complex, random microstructures. The effective fluid, gas, thermal, and electromagnetic transport properties of these materials play an important role in the large-scale dynamics and behavior of many geophysical systems. A striking feature of such media is that subtle changes in microstructural characteristics can induce changes over many orders of magnitude in the transport properties of the materials, which in turn can have significant large-scale geophysical effects. For example, sea ice, which mediates energy transfer between the ocean and atmosphere, plays a key role in global climate, and serves as an indicator of climatic change, is a porous composite of ice, brine and gases. Relevant length scales range from microns and millimeters for individual brine structures, to centimeters and meters for connected brine channels across floes, to hundreds of kilometers across an ice pack. Sea ice is distinguished from many other porous composites, such as sandstones or bone, in that its microstructure and bulk material properties can vary dramatically over a relatively small temperature range. The fluid permeability of sea ice ranges over six orders of magnitude for temperatures between 0°C and –25°C. Moreover, small changes in brine volume fraction around a threshold value of about 5%, corresponding to variations in temperature around a critical point of about –5°C, control an important transition between low and high fluid permeability regimes. Below this critical temperature, the sea ice is effectively impermeable, while for higher temperatures the brine phase becomes connected over macroscopic scales, allowing fluid transport through the ice. This transition has been observed to impact a wide range of phenomena such as surface flooding and snow–ice formation, enhancement of heat transfer due to fluid motion, mixing in the upper ocean, melt pool persistence, surface albedo (ratio of reflected to incident radiation) and other optical properties, growth and nutrient replenishment of algal and bacterial communities living in sea ice, and remote sensing of the sea ice pack from space. Recently, we have shown how continuum percolation theory can be used to understand the critical behavior of fluid transport in sea ice. Here we review this application of percolation theory to sea ice, and briefly discuss electromagnetic transport in sea ice, in particular how the geometry and connectivity of the brine microstructure determine its effective complex permittivity. © 2003 Elsevier B.V. All rights reserved.

*PACS:* 81.05.Rm; 47.55.Mh; 05.70.Jk; 93.30.Sq

*Keywords:* Sea ice; Percolation; Fluid permeability; Complex permittivity

---

## 1. Introduction

Composite materials made from two or more constituent media arise throughout the geophysical sciences. Rocks, soils, snow, sea ice and glacial ice are all examples of materials which display a

---

\*Fax: +801-581-4148.

*E-mail address:* [golden@math.utah.edu](mailto:golden@math.utah.edu) (K.M. Golden).

wide range of composite, random microstructures. How they interact with, and mediate interactions between, other components of geophysical systems is determined by their effective properties: fluid and gas permeability, thermal and electrical conductivity, optical and other electromagnetic transport properties, as well as mechanical properties. For example, sea ice is a composite of pure ice with brine and air inclusions, which mediates the exchange of heat, moisture, gases, momentum, and solar radiation between the ocean and atmosphere in the polar regions. As such, the polar sea ice covers play a key role in global climate and as an indicator of global climatic change [1,2]. They also play host to algal and other microbiological communities at the core of the polar oceanic food web [3,4]. Another example is the movement of fluids through rocks [5]. Fluid flow in the Earth's crust is especially important along active plate boundaries, where it can exert controlling effects on crustal rheology, deformation, seismicity and heat and mass transport. Much of this fluid flow has its origins in the inaccessible regions of the Earth's crust below the brittle–ductile transition, where metamorphism takes place, releasing large volumes of C–O–H-rich fluids. These fluids migrate through the rocks in response to buoyancy and deformation, transporting heat and mass, and producing chemical, isotopic, and mineralogical changes, including ore deposition. A third example is bubble trapping and the movement of air and gases through porous, glacial firn [6]. Below a critical depth zone, the air phase in ice from glaciers and the polar ice caps, is contained primarily in isolated bubbles disconnected from the atmosphere, which can be used in the analysis of past climate. In each example, the composite microstructure of the geophysical material controls the transport and other physical properties which can significantly impact geophysical dynamics and behavior on much larger scales.

Among geological, biological, and even engineered composite materials, sea ice is quite unique in that it naturally displays such a wide range of microstructures and transport properties over a relatively small range of temperatures and compositions. In particular, the geometry and statistical characteristics of the brine phase in sea ice depend

strongly on temperature, bulk salinity, and growth conditions. The connectivity of the brine phase over various length scales plays a key role in determining the effective fluid, thermal, and electromagnetic transport properties of sea ice. An interesting feature of sea ice, known to the earliest polar explorers, is its tendency to desalinate with time. Efforts to understand this fundamental process have led to many important discoveries about the microstructure and the dynamics of the brine phase. The dominant desalination mechanism has been found to be gravity drainage [7]. As an ice sheet grows, its surface rises higher above sea level, producing a pressure head in the interconnected brine system, driving the underlying brine out of the ice. In the presence of a temperature profile which increases with depth, an unstable density distribution exists within the brine, producing convective overturning, as well as an exchange between denser brine within the ice and the underlying seawater [7]. The input of brine into the upper ocean is important in ice–ocean interactions, through modification of the density of the surface layer, induction of thermohaline convection, and contributing to the formation of bottom water [8]. The drainage channels which facilitate brine transport consist of large, vertical tubular drainage structures attended by smaller tributaries, like a vertically oriented, radially symmetric river system [7].

One of the key findings which has resulted from the study of the desalination process is that for brine volume fractions  $p$  below a critical value  $p_c \approx 5\%$ , columnar sea ice is effectively impermeable to fluid transport, whereas for  $p$  above  $p_c$ , brine or sea water can move through the ice. The relation of brine volume to temperature  $T$  and salinity  $S$  [9] implies  $p_c$  corresponds to a critical temperature  $T_c \approx -5^\circ\text{C}$  for  $S = 5$  ppt (parts per thousand); we refer to this critical behavior as the “law of fives”. Perhaps its clearest demonstration in early works appears in Refs. [7,10], where the rate of change of salinity  $dS/dt$  due to gravity drainage is plotted against brine volume. For brine volumes below roughly 5%,  $dS/dt$  vanishes. Indeed, Ono and Kasai [11] have found that the downward permeability of thin sea ice decreases by over two orders of magnitude as the surface

temperature is lowered, in a small neighborhood of  $-5^{\circ}\text{C}$ .

Brine transport is fundamental to such processes as sea ice production through freezing of flooded ice surfaces [12], the enhancement of thermal fluxes through sea ice [13], nutrient replenishment for sea ice algal communities [4], and to remote sensing [14–16]. However, until recently the basic transition controlling brine transport has received little attention. Percolation theory [17,18] has been developed to analyze the properties of materials where connectedness of a given component determines the bulk behavior. Recently we have shown [19] that it provides a natural framework to understand the critical behavior of sea ice. In particular, we applied a compressed powder percolation model to sea ice microstructure that explains the law of fives, the observed behavior [11] of the fluid permeability in the critical temperature regime (qualitatively), as well as data on surface flooding collected on sea ice in the Weddell Sea and East Antarctic regions.

Other examples of brine percolation and transport include the observation in the Arctic [20] that a snow storm and its resultant loading can induce a complete upward flushing of the brine network. The freezing of a surface slush layer, with resultant brine drainage, was observed in the Antarctic to induce convection within the ice, whereby rejected dense brine is replaced by nutrient-rich sea water from the upper ocean [13], fueling autumn blooms of algae in second year ice [4]. During the autumn freeze-up, this process provided about 70% of the salt flux into the upper ocean and increased the total heat flux through the overlying ice and snow cover. Moreover, the proliferation and growth of sea ice organisms is favored in general by permeable ice which allows nutrient replenishment [21] for remote sensing, surface flooding and subsequent freezing can affect microwave backscatter from sea ice [14,15], and this surface flooding is often controlled by percolation processes. Moreover, the connectedness of the brine inclusions, as well as their volume fraction and geometry, affects the complex permittivity  $\epsilon^*$  of sea ice, which determines how electromagnetic waves are scattered from and propagate through the ice. We briefly discuss a series of rigorous bounds on the

effective complex permittivity  $\epsilon^*$  of sea ice [16,22,23], and how this theory can help in understanding the effective fluid and thermal transport properties of sea ice.

## 2. The percolation transition in sea ice

Percolation theory [17,18,24,25] was initiated with the introduction of a simple lattice model to study the flow of air through permeable sandstones used in miner's gas masks. In subsequent decades, this theory has been used to successfully model a broad array of disordered materials and processes, including flow in porous media like rocks and soils [26] various types of disordered conductors like piezoresistors, thermistors [27], radar absorbing composites [28], and polar firn [29]. The original percolation model and its generalizations have been the subject of intensive theoretical investigations, particularly in the physics [18,25] and mathematics [24] communities. One reason for the broad interest in the percolation model is that it is perhaps the simplest, purely probabilistic model which exhibits a type of phase transition.

The simplest form of the lattice percolation model [18] is defined as follows. Consider the  $d$ -dimensional integer lattice  $\mathbf{Z}^d$ , and the square (or cubic) network of bonds joining nearest neighbor lattice sites. To each bond, with probability  $p$ ,  $0 \leq p \leq 1$ , we assign a 1, meaning it is open, and with probability  $1 - p$  we assign a 0, meaning it is closed. Groups of connected open bonds are called open clusters, and the size of a cluster is just the number of open bonds it contains. In the percolation model there is a critical probability  $p_c$ ,  $0 < p_c < 1$ , called the percolation threshold, at which the average cluster size diverges and an infinite cluster appears, so that the open bonds percolate. In two dimensions  $p_c = 0.5$ , and in three  $p_c \approx 0.25$ . Typical open-cluster configurations in  $d = 2$  for  $p = \frac{1}{3}$  and  $p = \frac{2}{3}$  are shown in Fig. 1. For  $p \geq p_c$ , the infinite cluster density  $P_{\infty}(p)$ , defined as the probability that the origin (or any point, by translation invariance) is contained in the infinite cluster, or  $P_{\infty}(p) = \lim_{L \rightarrow \infty} M_{\infty}(L, p)/L^d$ , where  $M_{\infty}(L, p)$  is the mass of the infinite cluster

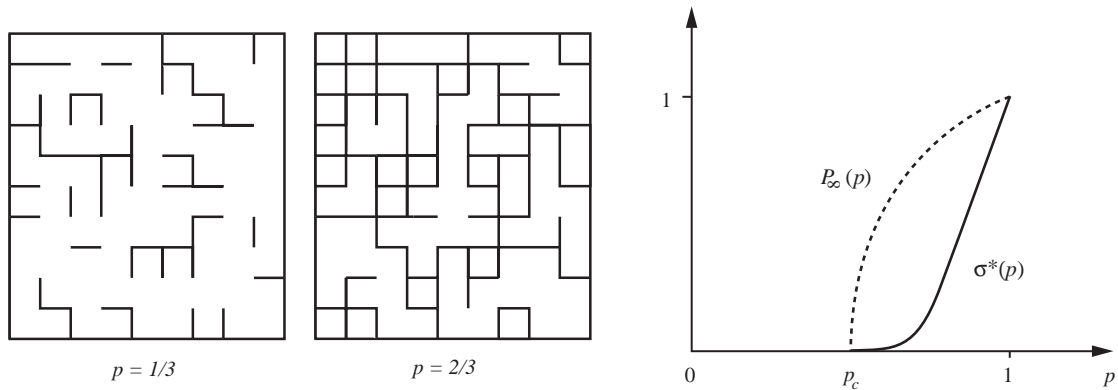


Fig. 1. Typical configurations of the two-dimensional lattice in bond percolation, below ( $p = \frac{1}{3}$ ) and above ( $p = \frac{2}{3}$ ) the percolation threshold  $p_c = \frac{1}{2}$ , and graphs of the infinite cluster density  $P_\infty(p)$  and effective conductivity  $\sigma^*(p)$ .

contained in a box of side  $L$ . At the percolation threshold, the infinite cluster has a self-similar, fractal structure, with  $M_\infty(L, p_c) \sim L^{d_f}$  as  $L \rightarrow \infty$ , where  $d_f \leq d$  is the fractal dimension. In two dimensions  $d_f = \frac{91}{48} \approx 1.9$  is a conjectured exact result, and  $d_f \approx 2.5$  in three dimensions [18,25]. The graph of  $P_\infty(p)$  for  $d = 2$  is shown in Fig. 1. In the neighborhood of  $p_c$ , with  $p \geq p_c$ ,  $P_\infty(p)$  is believed to exhibit the scaling behavior

$$P_\infty(p) \sim (p - p_c)^\beta, \quad p \rightarrow p_c^+, \quad (1)$$

where  $\beta$  is the percolation critical exponent, which satisfies  $\beta \leq 1$  [30], and in  $d = 2$  it is conjectured that  $\beta = 5/36$  [25].

The percolation model deals only with the geometrical aspects of connectedness in disordered media, yet we are interested in the transport properties as well. Then we consider a random resistor network, where the bonds are assigned the conductivities  $\sigma = 1$  and  $h \geq 0$  with probabilities  $p$  and  $1 - p$ . With  $h = 0$ , the effective conductivity  $\sigma^*(p)$ , obtained via solving Kirchoff's laws, vanishes for  $p < p_c$ ,  $\sigma^*(p) = 0$ .  $\sigma^*(p) > 0$  is believed to exhibit the power law behavior

$$\sigma^*(p) \sim (p - p_c)^t, \quad p \rightarrow p_c^+, \quad (2)$$

where  $t$  is the conductivity critical exponent, with  $1 \leq t \leq 2$  in  $d = 2, 3$  [31,32] and numerical values  $t \approx 1.3$  in  $d = 2$  and  $t \approx 2.0$  in  $d = 3$  [18]. The effective conductivity  $\sigma^*(p)$  in the  $d = 2$  lattice case is shown in Fig. 1. Analogously we may consider a random pipe network with effective

fluid permeability  $\kappa^*(p)$  exhibiting similar behavior  $\kappa^*(p) \sim (p - p_c)^e$ , where  $e$  is the permeability critical exponent, with  $e = t$  [26,32,33]. Such critical exponents, like  $t$  and  $e$ , are generally believed to exhibit universality, meaning that they depend only on dimension and not on the type of lattice, although continuum models can exhibit nonuniversal behavior, with exponent values different from the lattice case. For example, consider the Swiss cheese model in  $d = 2$ , where circular discs (or spheres in  $d = 3$ ) are removed at random from a uniform medium of unit (electrical or fluid) conductivity [18,34]. Near the percolation threshold, the transport properties are dominated by flow through the narrow necks between nonoverlapping discs (or spheres). Since the widths of such necks can vary throughout the system, there is a distribution of bond conductivities  $\sigma$  in an equivalent Voronoi network model. Moreover, this distribution is singular near  $\sigma = 0$ , which can lead to violations of universality with values of the transport critical exponents in  $d = 3$  higher than for the lattice case, and  $e \neq t$  [18,34].

If the above classical lattice percolation model is applied to sea ice, where the open bonds represent brine and the closed bonds represent ice, then  $p_c$  would be about 25% in  $d = 3$ , which is much larger than the observed 5%. Even continuum models, such as ellipsoidal brine inclusions randomly distributed in an ice host, a commonly used model for sea ice, exhibit critical volume fractions in the 20–40% range [35]. Instead consider the

critical behavior of composites made up of conducting particles suspended in an insulating matrix [27], and the problem of finding microstructures that reduce  $p_c$ . For some flexible polymer composites designed to be highly conducting, it was found that by compacting powders of large polymer particles with much smaller metal particles, microstructures exhibiting very low values of  $p_c$  could be obtained. Thus the amount of the more expensive metal particles required to significantly lower the resistance of the composite can be significantly lowered [36,37]. The resulting microstructure of such compressed powders is strikingly similar to the cellular microstructure of columnar sea ice, as shown in Fig. 2.

The key parameter in predicting the conduction threshold for compressed powders is the ratio  $\xi = R_p/R_m$  of the radii of the large polymer particles to the smaller metal particles [37,39]. An approximate, theoretical formula for the critical volume fraction for percolation of the small metal spheres in a compressed powder is given by

$$p_c = \left(1 + \frac{\xi\phi}{4x_c}\right)^{-1}, \quad (3)$$

where  $\phi$  is a reciprocal planar packing factor, and  $x_c$  is a critical surface area fraction of the larger particles which must be covered for percolation by the smaller particles [39]. Values based on microstructural analysis giving good agreement with conductivity experiments are  $x_c = 0.42$  and  $\phi = 1.27$  (which we use also as a reasonable approximation for sea ice). An alternative approach to approximating  $p_c$  which yields similar quantitative results can be found in Ref. [40]. For large  $\xi$ ,  $p_c$  is not very sensitive to the exact value of  $\xi$ . For example, a range of 44–17 in  $\xi$  gives only a range of 3–7% in  $p_c$ . Using photomicrographs of sea ice microstructure and typical brine inclusion sizes [7], we measured the corresponding parameter for sea ice, obtaining an average of  $\xi \approx 24$ . Applying the compressed powder percolation model [39] yields a critical brine volume for columnar sea ice of about 5%. This result will vary with ice crystal structure. For example, the slightly higher values of  $p_c$  (lower  $\xi$ ) observed in Ref. [11] are caused by the more random distributions of brine inclusions in granular ice as compared to columnar ice. The compressed powder model explains why sea ice exhibits such low values for  $p_c$ , as compared to

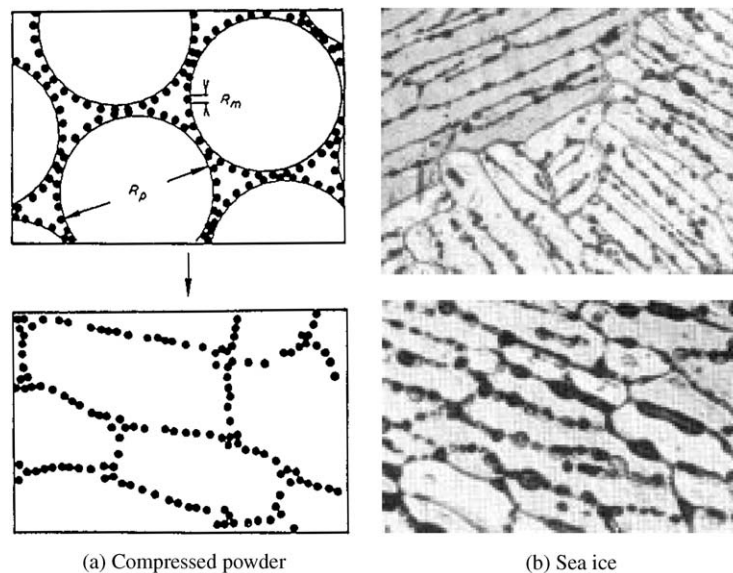


Fig. 2. Comparison of the microstructures of (a) compressed powder of large polymer particles of radius  $R_p$  and small metal particles of radius  $R_m$  [37], and (b) sea ice [38].

the 20% to 40% range one might expect, and provides reasonable estimates for  $p_c$ , which depends only on the geometry of the two phases.

Compressed powders with low  $p_c$  exhibit large, nonuniversal values of  $t$  ranging between 2 and 7 [27]. A rough estimate for the fluid permeability critical exponent  $e$  for sea ice based on the data in Ref. [11] is about 2.5, although there is significant uncertainty in this estimate (but  $e$  is probably between 2 and 4). Given that for lattice models we have shown in  $d = 3$  that  $e = t \leq 2$  [31], it is likely that sea ice exhibits nonuniversal behavior, perhaps indicating the importance of the very small necks through which brine must flow near the percolation threshold. Much more experimental work needs to be done to determine the actual range of  $e$ , how it depends on the type of sea ice and other factors, and if indeed the behavior is nonuniversal.

Data collected on Antarctic sea ice directly demonstrate the significance of the percolation threshold. During the winter ANZFLUX experiment [41] in the Eastern Weddell Sea we encountered a thin ice pack, typically 20–60 cm thick. Unusually large vertical oceanic heat fluxes resulted in ice basal melt rates of up to 3 cm/day (average was 1 cm/day) which could have melted the ice in a short period. The persistence of the ice depended on flooding of the surface and the subsequent freezing of this slushy snow/brine mixture to form snow ice, which replaced the ice melting on the bottom [12]. The surface flooding was controlled by upward brine percolation. Temperature profiles measured hourly during a 5-day drift camp over Maud Rise at about 4° E and 65° S indicated that while most of the sea ice layer remained above the critical temperature for percolation, the top 5 cm or so of the sea ice was impermeable, except during the typically warm storms. Sufficient loading led to surface flooding, which subsequently froze. This cyclic process occurred twice during the 5-day drift. The impermeable layer, defined by temperatures below a critical temperature of about  $-5.3^\circ\text{C}$ , disappeared with the onset of the first storm during day of year 216 (4 August 1994). For about a day the entire ice sheet was permeable, and by noon of the next day, we observed a thick layer of slushy snow

consisting of 30–50% liquid brine. Subsequently, a cold period set in, the slush froze, and the impermeable cap returned as the frozen slush. Then another storm moved in, with resultant warming, flooding, and freezing. Late in the evening of day 219 during a warm storm, we observed large “boils” on the snow surface, which was apparently brine percolating up through the ice.

Finally, consider the algae bloom observed in a porous sea ice layer at depth 10–30 cm during the autumn of 1992 in the Western Weddell Sea [4]. From day of year 60 (29 February) to 81 standing stocks of pigments in the ice were increasing at the rate of 0.8 mg/m/day, yet after day 81 the algal growth rate was reduced to one tenth the earlier value. Day 81 is when the downward advancing critical isotherm of  $T_c \approx -4^\circ\text{C}$  passed through the bottom of the algal layer, effectively cutting off the community from significant nutrient replenishment, as ice above this isotherm was impermeable. The critical temperature higher than  $-5^\circ\text{C}$  is understood by noting that the ice surrounding the algal layer was granular, and has a higher  $p_c$ , yet a salinity of only about 5 ppt.

### 3. Brine geometry and bounds on the complex permittivity of sea ice

In many cases of interest when considering the interaction of electromagnetic waves with sea ice, such as in remote-sensing applications, the wavelength is much longer than the millimeter scale of the brine inclusions. Then the quasistatic approximation is valid, and one considers the effective complex permittivity tensor  $\epsilon^*$  of the sea ice, or a diagonal coefficient within the horizontal plane for example, denoted by  $\epsilon^*$ . Due to the wide variety of possible microstructures and the high dielectric contrast of the components of brine and ice, it is in general quite difficult to accurately predict the effective complex permittivity  $\epsilon^*$  for sea ice, although many “mixing formulas” for  $\epsilon^*$  have been proposed and compared with experimental data, e.g. Refs. [42–44], where typically the sea ice is assumed to consist of a host of pure ice containing ellipsoidal brine and air inclusions.

While mixing formulas are certainly useful, their applicability to the full range of microstructures presented by sea ice is limited, and the assumptions under which they are derived are not always satisfied, such as when the brine inclusions percolate. Consequently, we have developed [16,22] a comprehensive series of rigorous bounds on  $\varepsilon^*$  for sea ice, valid in the quasistatic regime, which we briefly describe. The sea ice is assumed to be a two-component, stationary random, composite medium of brine with complex permittivity  $\varepsilon_1$  depending on frequency and temperature, and ice of permittivity  $\varepsilon_2$ , depending weakly on frequency and temperature ( $\varepsilon_2$  is slightly adjusted via the Maxwell–Garnett formula to account for the presence of air [16,45]). Our approach is based on a general, analytic continuation method for obtaining bounds on the effective properties of composites [46–48], where  $\varepsilon^*$  is treated as an analytic function of  $h = \varepsilon_1/\varepsilon_2$ , and its properties are exploited to obtain the bounds, which apply to any two component medium, such as snow or slush, which are also of interest for sea ice remote sensing. A full treatment of composites with three or more components is more involved mathematically, requiring analysis of holomorphic functions of several complex variables [49,50].

The effective complex permittivity tensor  $\varepsilon^*$  is defined via

$$\langle D \rangle = \varepsilon^* \langle E \rangle, \quad (4)$$

where  $E$  and  $D$  are the stationary random electric and displacement fields satisfying  $D = \varepsilon E$ , with  $\varepsilon(x), x \in \mathbf{R}^d$ , the local complex permittivity taking values  $\varepsilon_1$  and  $\varepsilon_2$ ,  $\nabla \cdot D = 0$ , and  $\nabla \times E = 0$ . The notation  $\langle \cdot \rangle$  means ensemble average over realizations of the random medium, or spatial average over all of  $\mathbf{R}^d$ .

The key step in the method is to obtain the Stieltjes integral representation [46–48]

$$F(s) = 1 - \varepsilon^*/\varepsilon_2 = \int_0^1 \frac{d\mu(z)}{s - z}, \quad s = (1 - \varepsilon_1/\varepsilon_2)^{-1}, \quad (5)$$

where  $\mu$  is a positive (spectral) measure on  $[0, 1]$  containing all the information about the geometry of the composite, which is separated from the parameter information contained in  $s = 1/(1 - h)$ .

Statistical information about the geometry is input through the moments  $\mu_n$  of  $\mu$ , which are related to the correlation functions of the brine phase. For example,  $\mu_0 = p_1$ , the volume fraction of brine. Bounds on  $\varepsilon^*$ , or  $F(s)$ , are obtained by fixing  $s$  in (5), varying over admissible measures  $\mu$  (corresponding to admissible geometries), such as those that satisfy only  $\mu_0 = p_1$ , and finding the corresponding range of values of  $F(s)$  in the complex plane. If just  $p_1$  is known, we obtain a region  $R_1$  in the complex  $\varepsilon^*$ -plane, in which the complex permittivity of sea ice of that brine volume must lie, regardless of geometry. If the sea ice microstructure is further assumed to be isotropic within the horizontal plane, we obtain a smaller region  $R_2$  [47].

If we further assume that the sea ice is a matrix–particle composite, where the brine phase is contained in separated inclusions, there is a spectral gap — that is, the support of  $\mu$  in Eq. (5) lies in an interval  $[s_m, s_M]$ ,  $0 < s_m < s_M < 1$ , as observed in fundamental work by Bruno [51]. The further the separation of the inclusions, the smaller the support interval  $[s_m, s_M]$ , or the larger the spectral gap, and the tighter the bounds. We obtain regions  $R_1^{\text{mp}}$  and  $R_2^{\text{mp}}$  which are significant improvements over  $R_1$  and  $R_2$  [16]. To compare the matrix-particle bounds with data in [38], we assume that within the horizontal plane, the brine is contained in separated, circular discs, which allows us to utilize the explicit calculations in [51] of  $s_m$  and  $s_M$ . In particular, we consider discs of brine of radius  $r_b$  which hold random positions in a host of ice, in such a way that each disc of brine is surrounded by a “corona” of ice, with outer radius  $r_i$ . Then the minimal separation of brine inclusions is  $2(r_i - r_b)$ . Such a medium is called a  $q$ -material, where  $q = r_b/r_i$ ,  $0 < q < 1$ . For such a geometry, Bruno has calculated [51]  $s_m = \frac{1}{2}(1 - q^2)$  and  $s_M = \frac{1}{2}(1 + q^2)$ . Smaller  $q$  values indicate well-separated brine (and presumably cold temperatures), and  $q = 1$  corresponds to no restriction on the separation, with  $s_m = 0, s_M = 1$ , so that  $R_1^{\text{mp}}$  and  $R_2^{\text{mp}}$  reduce to  $R_1$  and  $R_2$ . Examination of photomicrographs of the brine microstructure in the sea ice samples of [36] indicates that even when the ice is quite cold, the brine inclusions are quite close, and it is very difficult to estimate

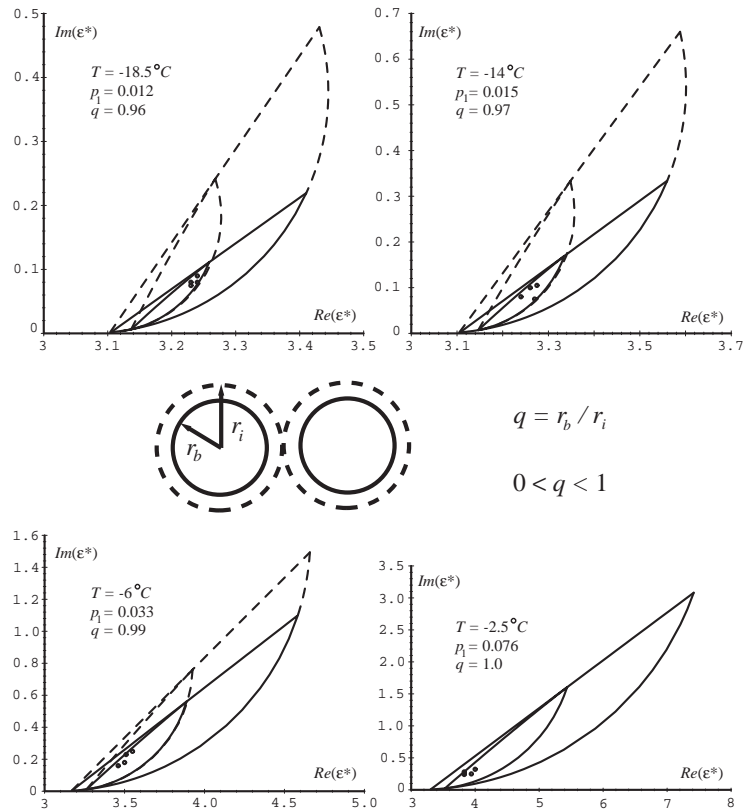


Fig. 3. Comparison of 4.75 GHz data (circles) on the complex permittivity  $\epsilon^*$  of sea ice at different temperatures [36] with the bounds  $R_1$  (outer, dotted),  $R_2$  (inner, dotted),  $R_1^{\text{mp}}$  (outer, solid), and  $R_2^{\text{mp}}$  (inner, solid).  $R_1$  assumes knowledge of the brine volume and  $R_2$  assumes statistical isotropy as well.  $R_1^{\text{mp}}$  and  $R_2^{\text{mp}}$  further assume that the sea ice is a matrix–particle composite with the indicated  $q$  values corresponding to the geometry in the diagram. For  $T = -2.5^\circ\text{C}$  the matrix–particle assumption is no longer valid,  $q = 1$ , and  $R_1^{\text{mp}}$  and  $R_2^{\text{mp}}$  reduce to  $R_1$  and  $R_2$ .

appropriate values of  $q$ . Instead, for a given data set at a particular temperature, we choose a value of  $q$  which best captures the data, and it is always quite close to 1. Computationally we find that because of the high contrast in the components, the bounds  $R_1^{\text{mp}}$  and  $R_2^{\text{mp}}$  are extremely sensitive to small changes in  $q$  for  $q$  near 1. This is a reflection of a potential percolation threshold there, with a corresponding large transition in the values of  $\epsilon^*$ . By carefully comparing our bounds to data over a wide range of temperatures, we have found that as the temperature increases, i.e., as the percolation threshold  $T_c$  is approached and the brine inclusions grow closer, the data sweep across from one side of the region  $R_2$  to the other (while the regions becomes larger as the brine volume increases), and

$q$  increases as well. Once the temperature is above  $T_c$ , the data require that  $q = 1$ , and the matrix–particle assumption is no longer valid. This fascinating behavior is illustrated in Fig. 3, which compares data from samples 84-3 and 84-4 ( $S = 3.8$  ppt) in Ref. [36] with the bounds as the temperature is varied over a wide range.

In closely related work [23,45], enlarging upon previous work of McPhedran and Milton [52], we have developed a rigorous theory of inverse homogenization, based on inversion of the bounds  $R_1$  and  $R_2$ , which has produced an accurate algorithm for reconstructing the brine volume of sea ice from measurements of the effective complex permittivity. Moreover, through more sophisticated mathematical techniques, with C. Orum and

E. Cherkaev, we have inverted the matrix particle bounds  $R_1^{\text{mp}}$  and  $R_2^{\text{mp}}$  as well to obtain inverse bounds on the separation parameter  $q$  from measurements of  $\varepsilon^*$ . Finally, in forthcoming works we shall employ percolation theory and various types of bounds to study the fluid permeability and thermal conductivity of sea ice, and their relations.

### Acknowledgements

The author would like to thank Steve Ackley and Vicky Lytle for their many contributions to the development of this work. The author is also grateful for the support provided by NSF Grants OPP-97-25038 and DAS-02-22171.

### References

- [1] N. Untersteiner (Ed.), *The Geophysics of Sea Ice*, Plenum Press, New York, 1986.
- [2] M.O. Jeffries (Ed.) *Antarctic Sea Ice: Physical Processes, Interactions and Variability*, American Geophysical Union, Washington, DC, 1998.
- [3] M.P. Lizotte, K.R. Arrigo (Eds.), *Antarctic Sea Ice: Biological Processes, Interactions and variability*, American Geophysical Union, Washington, DC, 1998.
- [4] C.H. Fritsen, V.I. Lytle, S.F. Ackley, C.W. Sullivan, *Science* 266 (1994) 782.
- [5] W.S. Fyfe N.J. Price, A.B. Thompson, *Fluids in the Earth's Crust*, Elsevier, New York, 1978.
- [6] I.G. Enting, *Nature* 315 (1985) 654.
- [7] W.F. Weeks, S.F. Ackley, *The Growth, Structure and Properties of Sea Ice*, Monograph, 82–1, USA CRREL, Hanover, NH, 1982.
- [8] E.C. Carmack, *Circulation and mixing in ice-covered waters*, in: N. Untersteiner (Ed), *The Geophysics of Sea Ice*, Plenum Press, New York, 1986, p. 641–712.
- [9] G. Frankenstein, R. Garner, *J. Glaciol.* 6 (48) (1967) 943.
- [10] G.F.N. Cox, W.F. Weeks, *Brine drainage and initial salt entrapment in sodium chloride ice*, Research Report 354, USA CRREL, Hanover, NH, 1975.
- [11] N. Ono, T. Kasai, *Ann. Glaciol.* 6 (1985) 298.
- [12] S.F. Ackley, V.I. Lytle, K.M. Golden, M.N. Darling, G.A. Kuehn, *Antarct. J.U.S.* 30 (1995) 133.
- [13] V.I. Lytle, S.F. Ackley, *J. Geophys. Res.* 101 (C4) (1996) 8853.
- [14] A.R. Hosseinmostafa, V.I. Lytle, K.C. Jezek, S.P. Gogineni, S.F. Ackley, R.K. Moore, *J. Electromagnetic Appl.* 9 (1995) 421.
- [15] V.I. Lytle, K.M. Golden, *Antarctic J.U.S.* 30 (1995) 125.
- [16] K.M. Golden, *The interaction of microwaves with sea ice*, in: G. Papanicolaou, (Ed), *Wave Propagation in Complex Media*, IMA Volumes in Mathematics and its Applications, Vol. 96, Springer, Berlin, 1997, p. 75–94.
- [17] S.R. Broadbent, J.M. Hammersley, *Proc. Cambridge Philos. Soc.* 53 (1957) 629.
- [18] D. Stauffer, A. Aharony, *Introduction to Percolation Theory*, 2nd Edition, Taylor & Francis, London, 1992.
- [19] K.M. Golden, S.F. Ackley, V.I. Lytle, *Science* 282 (1998) 2238.
- [20] E.J.-J. Hudier, R. G. Ingram, *Atmosphere-Ocean* 33 (1995) 569.
- [21] G.S. Dieckmann, M.A. Lange, S.F. Ackley, J.C. Jennings, *Polar Biol.* 11 (7) (1991) 449.
- [22] K. Golden, *J. Geophys. Res. (Oceans)* 100 (C7) (1995) 13,699.
- [23] K.M. Golden, D. Borup, M. Cheney, E. Cherkaeva, M. S. Dawson, K.H. Ding, A.K. Fung, D. Isaacson, S.A. Johnson, A.K. Jordan, J.A. Kong, R. Kwok, S.V. Nghiem, R.G. Onstott J. Sylvester, D.P. Winebrenner, I. Zabel, *IEEE Trans. Geosci. Remote Sensing* 36 (5) (1998) 1675.
- [24] G. Grimmett, *Percolation*, Springer, New York, 1989.
- [25] A. Bunde, S. Havlin, (Eds.), *Fractals and Disordered Systems*, Springer, New York, 1991.
- [26] M. Sahimi, *Flow and Transport in Porous Media and Fractured Rock*, VCH, Weinheim, 1995.
- [27] D.S. McLachlan, M. Blaszkiewicz, R.E. Newnham, *J. Am. Cream. Soc.* 73 (8) (1990) 2187.
- [28] A. Priou (Ed.), *Dielectric Properties of Heterogeneous Materials*, Elsevier, New York, 1992.
- [29] S. Shabtaie, C.R. Bentley, *J. Geophys. Res.* 99 (B10) (1994) 19,757.
- [30] J.T. Chayes, L. Chayes, *Phys. Rev. Lett.* 56 (1986) 1619.
- [31] K. Golden, *Phys. Rev. Lett.* 65 (24) (1990) 2923.
- [32] K.M. Golden, *Percolation models for porous media*, in: U. Hornung, (Ed). *Homogenization and Porous Media*, Springer, New York, 1997, p. 27–43.
- [33] J.T. Chayes, L. Chayes, *Commun. Math. Phys.* 105 (1986) 133.
- [34] B.I. Halperin, S. Feng, P.N. Sen, *Phys. Rev. Lett.* 54 (22) (1985) 2391.
- [35] S. DeBondt, L. Froyen, A. Deruyttere, *J. Mater. Sci.* 27 (1992) 1983.
- [36] R.P. Kusy, D.T. Turner, *Nature* 229 (1971) 58.
- [37] A. Malliaris, D.T. Turner, *J. Appl. Phys.* 42 (2) (1971) 614.
- [38] S.A. Arcone, A.J. Gow, S. McGrew, *J. Geophys. Res.* 91 (C12) (1986) 14281.
- [39] R.P. Kusy, *J. Appl. Phys.* 48 (12) (1977) 5301.
- [40] J. Janzen, *J. Appl. Phys.* 51 (4) (1980) 2279.
- [41] M.G. McPhee, S.F. Ackley, P. Guest, B.A. Huber, D.G. Martinson, J.H. Morison, R.D. Muench, L. Padman, T.P. Stanton, *Bull. Am. Met. Soc.* 77 (1996) 1221.
- [42] P. Hoekstra, P. Capillino, *J. Geophys. Res.* 76 (20) (1971) 4922.

- [43] K.M. Golden, S.F. Ackley, *J. Geophys. Res. (Oceans)* 86 (C9) (1981) 8107.
- [44] A. Stogryn, *IEEE Trans. Geosci. Remote Sensing* GE-25 (2) (1985) 147.
- [45] E. Cherkaeva, K.M. Golden, *Waves Random Media* 8 (4) (1998) 437.
- [46] D.J. Bergman, *Phys. Rep. C* 43 (9) (1978) 377.
- [47] G.W. Milton, *Appl. Phys. Lett.* 37 (1980) 300.
- [48] K. Golden, G. Papanicolaou, *Commun. Math. Phys.* 90 (1983) 473.
- [49] K. Golden, *J. Mech. Phys. Solids* 34 (4) (1986) 333.
- [50] G.W. Milton, *Commun. Math. Phys.* 111 (281–327) (1987) 329.
- [51] O. Bruno, *Proc. R. Soc. London A* 433 (1991) 353.
- [52] R.C. McPhedran, G.W. Milton, *Matter Res. Soc. Symp. Proc.* 195 (1990) 257.